Determining the ion temperature and energy distribution in a lithium-plasma interaction test stand with a retarding field energy analyzer

M. Christenson, S. Stemmley, S. Jung, J. Mettler, X. Sang, D. Martin, K. Kalathiparambil, and D. N. Ruzic

Citation: Review of Scientific Instruments **88**, 083501 (2017); doi: 10.1063/1.4995601
View online: https://doi.org/10.1063/1.4995601
View Table of Contents: http://aip.scitation.org/toc/rsi/88/8
Published by the American Institute of Physics

Determining the ion temperature and energy distribution in a lithium-plasma interaction test stand with a retarding field energy analyzer

M. Christenson, S. Stemmley, S. Jung, J. Mettler, X. Sang, D. Martin, K. Kalathiparambil, and D. N. Ruzic
Department of Nuclear Plasma and Radiological Engineering, University of Illinois at Urbana-Champaign, Urbana, Illinois 61801, USA

(Received 6 March 2017; accepted 9 July 2017; published online 1 August 2017)

The ThermoElectric-driven Liquid-metal plasma-facing Structures (TELS) experiment at the University of Illinois is a gas-puff driven, theta-pinch plasma source that is used as a test stand for off-normal plasma events incident on materials in the edge and divertor regions of a tokamak. The ion temperatures and resulting energy distributions are crucial for understanding how well a TELS pulse can simulate an extreme event in a larger, magnetic confinement device. A retarding field energy analyzer (RFEA) has been constructed for use with such a transient plasma due to its inexpensive and robust nature. The innovation surrounding the use of a control analyzer in conjunction with an actively sampling analyzer is presented and the conditions of RFEA operation are discussed, with results presented demonstrating successful performance under extreme conditions. Such extreme conditions are defined by heat fluxes on the order of 0.8 GW m^{-2} and on time scales of nearly 200 μs. Measurements from the RFEA indicate two primary features for a typical TELS discharge, following closely with the pre-ionizing coaxial gun discharge characteristics. For the case using the pre-ionization pulse (PiP) and the theta pinch, the measured ion signal showed an ion temperature of 23.3 ± 6.6 eV for the first peak and 17.6 ± 1.9 eV for the second peak. For the case using only the PiP, the measured signal showed an ion temperature of 7.9 ± 1.1 eV for the first peak and 6.6 ± 0.8 eV for the second peak. These differences illustrate the effectiveness of the theta pinch for imparting energy on the ions. This information also highlights the importance of TELS as being one of the few linear pulsed plasma sources whereby moderately energetic ions will strike targets without the need for sample biasing. *Published by AIP Publishing.* [http://dx.doi.org/10.1063/1.4995601]

I. INTRODUCTION

Detrimental events at the plasma-material boundary in the edge region of a tokamak have given rise to a bolstered research effort regarding confinement, energy deposition, and plasma-material interactions. Disruptions and edge-localized modes (ELMs) result in very high energy ions bombarding edge material surfaces over a very brief time scale. ITER ELMs are predicted to deposit power densities on the order of 1 GW m^{-2} over the duration of 0.1–0.5 ms.[1] A recent report estimates that the plasma facing components in the ITER will not be able to tolerate such high levels of energy deposition unless the ELM energies are reduced by 95% or the ELMs are eliminated altogether.[2] Therefore, effort has been placed in modifying the frequency and energy of ELM events along with developing novel concepts for more robust plasma facing materials.

Studies at the University of Illinois have been aimed at overcoming these challenges. By utilizing the heat gradient established within thin trenches running along a structural support material in combination with an external magnetic field, the Lithium-Metal Infused Trenches (LiMIT) device can maintain a passive liquid lithium flow due to a generated thermoelectric magnetohydrodynamic force.[3] Apart from the fact that it is a low-Z material, lithium has been selected as the medium of choice for these experiments due to its ability to produce less radiative losses than tungsten or carbon, getter impurities such as carbon and oxygen, and generate lower recycling coefficients.[4,5] Along with these benefits, flowing liquid lithium would aid in reducing damage to the wall and divertor incurred by ELMs and disruptions. ThermoElectric-driven Liquid-metal plasma-facing Structures (TELS)[6–9] have been used in tandem with LiMIT tests performed in the Solid/Liquid Lithium Divertor Experiment (SLiDE) in order to further investigate the order-of-magnitude ELM-like events incident on a flowing liquid lithium surface, as well as illuminate the issues surrounding lithium vapor shielding.[9]

In order to accurately assess the level of event simulation and fully appreciate the mechanism by which energy is deposited on the surface of target materials in TELS, priority has been placed on measuring the ion temperatures and resultant energy distributions in the highly transient plasma. TELS plasmas are important in plasma-facing component research since the adiabatic compression of its theta pinch preferentially imparts energy to the ions, giving the TELS device the ability to mimic transient events with energetic ions without biasing the sample. While measurements of ion parameters are rare within the edge and scrape-off layers of fusion devices, retarding field energy analyzers (RFEAs) have been shown to be successful under these extreme conditions.[10–13] However, these analyzers have operated with plasmas bearing quasi-steady state characteristics, with pulse times lasting on the order of tens to hundreds of milliseconds. Typical pulse lengths for TELS are

on the order of 200 μs, which give rise to physical phenomena that are otherwise neglected in analogous quasi-steady state and steady state systems. It is because of these phenomena that a control analyzer was used as a means to accurately assess measurements.

This paper presents the development, operation, and results of an RFEA used to characterize ion behavior within a transient plasma generated by the TELS system. Section II describes the principal elements of the TELS and RFEA devices while focusing primarily on the RFEA. Section III explains the underlying physics governing RFEA operation. Section IV details the initial results from successful RFEA operation in the forms of ion temperature and distribution function analysis. Section V summarizes the results and describes future experimental work.

II. RFEA DESCRIPTION AND OPERATION

To understand the information collected by the RFEA, the TELS device (Fig. 1) will be briefly described. A more thorough description can be found in Ref. 8. Over a pulsed plasma duration of 150–200 μs, the power delivered to a target ranges on the order of 0.2–0.8 GW m^{-2} with an electron density ranging from 1×10^{20} m^{-3} to 1×10^{21} m^{-3} and an electron temperature between 20 and 50 eV, depending on the discharge conditions.[8] Representative TELS discharge currents are plotted in Fig. 3, which are also typical for all reported experiments during which the theta pinch is used. All experiments discharged a −5.5 kV potential through the PiP. Experiments that used the theta pinch discharged a 16.5 kV potential across the 1° conical set of theta coils used for confinement and compression. The inner diameter of the coil varies axially due to the conical shaping, but is 0.1 m on average, which surrounds a Pyrex tube. TELS uses a puff-gas valve in conjunction with a coaxial plasma accelerator to pre-ionize the gas and accelerate it toward the theta pinch at a high velocity, measured

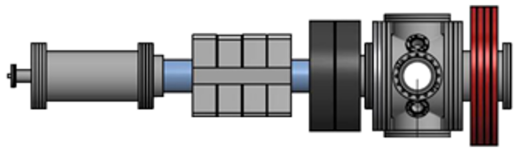

FIG. 1. An autodesk inventor image of the entire TELS chamber.[8] The coaxial gun chamber is on the left, while the target chamber sits to the right. The light gray blocks in the center are the theta pinch coils. Surrounding the target chamber are the "gray" and "copper" guiding magnets, which remain unused for the experiments reported herein. The plasma propagates from the coaxial gun chamber on the left to the target chamber on the right, in which is mounted the RFEA assembly. Reprinted with permission from S. Jung, "Development of high energy pulsed plasma simulator for plasma-lithium trench experiment," Ph.D. dissertation (University of Illinois at Urbana-Champaign, 2014).

between 24 and 40 km s^{-1},[8] using the intrinsically generated ***J x B*** force. This plasma shock front is highly ionized and highly collisional. The strength of the fringing field caused by the theta pinch in the target chamber ranges between 0.01 and 0.03 T and is dominated by the B_z component.

A physical depiction of the RFEA can be seen in Fig. 2, which consists of an inlet collimating slit measuring 5 μm × 3 mm laser machined into a tungsten disk, purchased from Lenox Laser (d = 9.5 mm and t = 0.025 mm for diameter and thickness, respectively), three stainless steel grids of various mesh size for potential sweeping, and a copper plate for current collection (d_{plate} = 22.2 mm and t_{plate} = 1.27 mm for diameter and thickness, respectively). The device is similar in design to that found in Ref. 10. The summation of the transparency factors for the individual grids and the collimating slit leads to an overall transparency factor for the analyzer system which is on the order of 2×10^{-4} %. The grids are isolated from each other using glass-mica. These washers maintain a uniform distance between the grids of 1.651 mm. The RFEA system is mounted in a 430 ferritic steel enclosure. Two analyzers were mounted normal to the plasma drift flow and magnetic field on a linear motion feed through, one open to incoming plasma

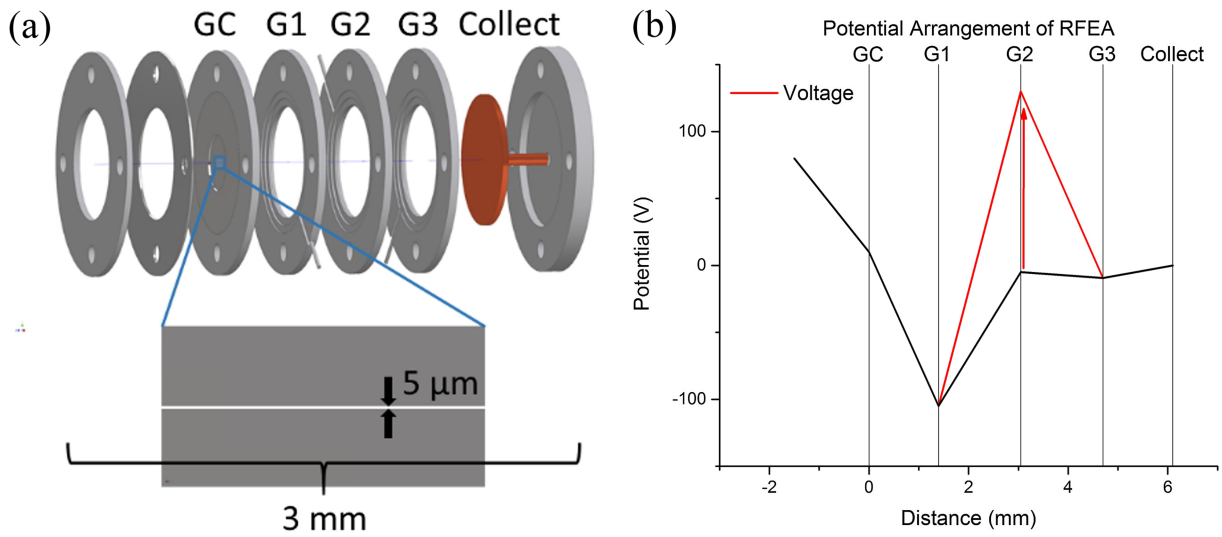

FIG. 2. (a) An exploded inventor image of the analyzer body. An expanded/highlighted view of the collimating slit is also shown. Distances between grids are (1) GC → G1 = 1.384 mm, (2) G1 → G2 = 1.651 mm, (3) G2 → G3 = 1.651 mm, and (4) GC → Collect = 1.397 mm. (b) The potential arrangement in an individual RFEA. A distance of 0 mm corresponds to the collimating plate.

flow and one closed off from the plasma using a Teflon shield to act as a control.

Since TELS plasmas are highly transient with pulse times between 150 and 200 μs, the collection of a characteristic current waveform from the RFEA collector required measurement on a shot-to-shot basis. The initial electron-repelling grid was held at −105 Vdc for shots using the theta pinch and −59 Vdc for shots without the theta pinch. This was done to sweep out the remaining electrons able to make it past the initial collimating aperture. The ion retarding grid was varied between −5 and 120 Vdc using a KEPCO ATE 150-3.5M DC power supply, with five BHC Aerovox 330 μF capacitors connected to each other in parallel and connected to the output of the power supply. The final electron-repelling grid used to prevent secondary emission backflow was held at −9.4 Vdc. The initial aperture was left floating to establish a well-defined sheath potential drop, while the collector was held at power ground. Power provided to the ion discriminating grid was in reference to power ground. All potentials were delivered and maintained using RG-58 coaxial cables from an isolated Faraday cage to the Bayonet Neill-Concelman (BNC) feedthroughs. Currents for each analyzer were collected and monitored on an Agilent Infiniium oscilloscope using two Tektronix P5200 high voltage differential probes measured across separate 10 kΩ resistors.

III. THEORY OF OPERATION

A. General theory

The underlying principles for RFEA measurement are described in Ref. 17. Charged particles enter through an initial aperture or grid, in an attempt to collimate the incoming flux, and are met with retarding fields that are maintained by biasing a sequential series of grids. Since TELS is a magnetized linear device, care was taken to orient the analyzer to sample the particles traveling axially, parallel to the direction of the magnetic field through the target chamber. The entrance aperture was chosen to be on the order of the Debye length ($\lambda_D = \sqrt{\varepsilon_0 k_B T/ne^2}$, typically 3 ± 1.5 μm for TELS plasmas) to ensure that the plasma did not fully penetrate into the device and to establish a well-defined sheath drop through which incoming ions are accelerated.

The characteristic current-voltage relationship corresponds to an integral of the ion velocity parallel to the magnetic field,[13]

$$I_C = A_{open} eZ \int_{\sqrt{|2eV_0/m|}}^{\infty} \varepsilon f_\infty(v_\infty) v_\infty dv_\infty, \tag{1}$$

where A_{open} is the area of the initial aperture, Z is the effective ion charge, ε is the system ion transmission factor, V_0 is the ion retarding bias, v_∞ is $-\sqrt{|2eV_0/m|}$, and $f_\infty(v_\infty)$ is the resulting distribution. The velocity distribution in TELS can be closely approximated as a shifted Maxwellian with regards to the sheath potential, due in large part to the fact that TELS plasmas have a high degree of ionization and are highly collisional, with characteristic collision times being much less than the transit time of the bulk plasma. These characteristics have been observed and reported for a number of similar Marshall-type coaxial plasma accelerators.[14–16] The functional form of the I-V relationship is given as follows:[13,17]

$$I_C = \begin{cases} I_0, & V_0 < V_s \\ I_0 \exp\left[-\dfrac{Z(V_0 - V_s)}{T_i}\right], & V_0 \geq V_s \end{cases}, \tag{2}$$

where $I_0 = A_{aperture}\, q_i \varepsilon$ is the effect of current directed on the collector without retarding bias and $V_s = V_p - V_c$ or the shift potential resulting from the difference of the collector potential from the plasma potential. Experimental data were fit to Eq. (2) to determine the shift potential and the initial current. Fitting the normalized derivative of the collected current, I_C, with respect to the discriminating potential, V_0, to a Maxwellian distribution in energy was done to evaluate the ion temperature. For all analyses, the ion charge was assumed for a pure plasma without any significant level of impurities.

B. Electromagnetic effects

Unlike a number of other studies that have used electrostatic analyzers to extract ion information from either low or high temperature plasmas, the analyzer in TELS is subject to a repeated number of highly transient, energetic events. Two effects from electromagnetic effects are the cause for noise being observed in both the collection and transmission lines. The first effect is a result of induction current since the transmission lines and collector may be subjected to a time-varying magnetic field. The first effect can be easily deduced from Faraday's law of induction, otherwise known as the Maxwell-Faraday equation. In the case of TELS, both the analyzer grids and transmission lines are subjected to a time-varying magnetic field that propagates axially down the length of the chamber. Approximating that the magnetic field profile is similar to the theta pinch profile, shown in Fig. 3(a), the peak theta pinch current yields a peak magnetic field of 300 G in the target chamber. The resulting pulse-averaged induced electromotive force (EMF) on an unshielded wire loop measuring 0.2 mm in diameter and 0.457 m in length is approximately 5.4×10^{-3} V, resulting in an overall induced current of nearly 11 mA. Since the RFEA body and collector are mounted inside 430 ferritic steel enclosure, the magnetic field permeation area is likely that of the entrance collimating slit, measuring 3 mm × 5 μm. The mean induced EMF is 8.1×10^{-7} V, which yields a 1.6 μA current. While the induced current on the collector is negligible, the induced current on the extreme case of an unshielded transmission line is substantial. In most systems, cables and diagnostics are shielded, which is true also in the case of the TELS RFEA. However, especially where there exists improper coverage of the sensitive diagnostics or cabling, inductive effects may still plague the system. The need for a control analyzer to help deduce the magnitude to which this phenomenon affects measurements is vital for pulsed systems like TELS.

The second electromagnetic effect that perturbs the collected currents is due to the rapid time scales associated with displacement currents in Maxwell's relation that describes the curl of the magnetic field,

$$\nabla \times \boldsymbol{B} = \mu_0 \left(\boldsymbol{J} + \varepsilon_0 \frac{\partial E}{\partial t} \right), \tag{3}$$

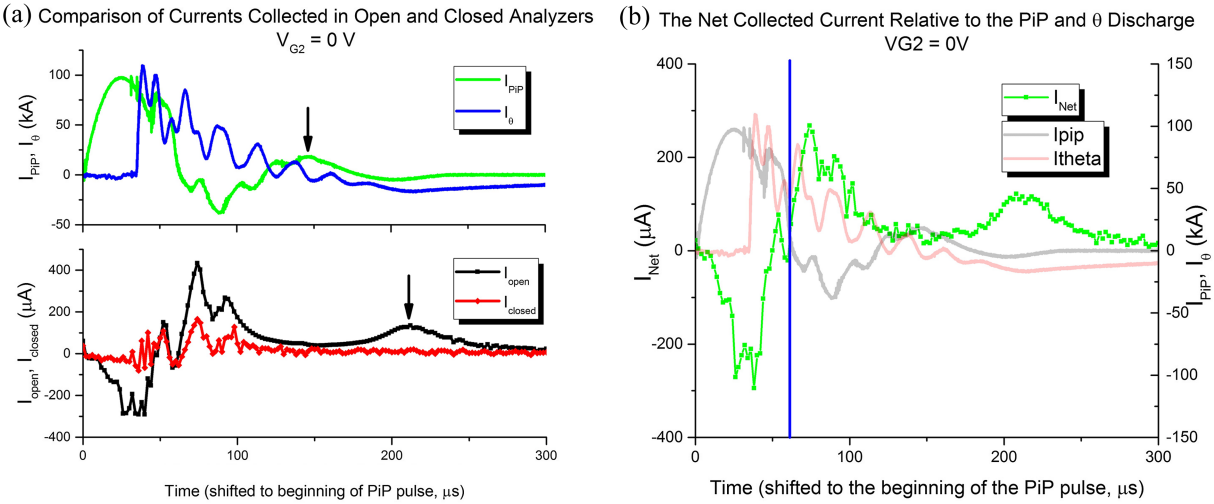

FIG. 3. (a) The collected currents of the control and open analyzers relative to the PiP and θ pinch discharge currents. The black arrows relate the secondary feature observed during RFEA current collection to the portion of the PiP discharge profile responsible for this feature. (b) The net current found from the difference in the current between the two analyzers. TELS plasma velocities from Ref. 8 indicate that the transit time from the PiP to the target chamber aligns with the vertical line in (b) at 61 μs.

where μ_0 is the vacuum permeability, ε_0 is the vacuum permittivity, and $\boldsymbol{J}$ is the free current density. In steady-state and even semi-transient events, the displacement current governed by the time-varying electric field is often ignored due to its negligible contribution to the curl of the magnetic field, and vice versa. In the case of TELS, however, not only do the effects of a highly transient magnetic field induce currents that can perturb transmission and collection in the analyzer and along transmission lines, but these effects are also coupled with the highly transient nature of the electric field as well. It is much more of a challenge to approximate perturbations, even to the zeroth order, of the time-varying electric field in the TELS device because the nature of the pulse itself is oscillatory, both at the fundamental and harmonic frequencies. As a worst-case-scenario estimate, one can assume that if the PiP pulse discharges all of the energy held in the coaxial accelerator capacitors (5.5 kV) and the radial distance from cathode to anode is 3.81 cm, then the peak electric field of the discharge felt in the target region never reaches above 1.4×10^5 V m^{-1}, assuming of course that there was no major contribution from the theta pinch. Differentiating the electric field profile of the PiP with respect to time, multiplying by the electric permittivity and the affected area, the maximum displacement current that can affect the transmission cables is 3.8×10^{-4} A, with 5.7×10^{-8} A being the maximum displacement current felt by the collector. This means that, in general, the effects of induction are much more serious than the effects of displacement current and must be properly accounted for using the control analyzer and proper shielding. It is interesting to note, however, that the maximum current collected by the closed analyzer in Fig. 3(a) is slightly less than 200 μA, which may in fact be related to the effects that displacement current has on the transmission and collection lines. The importance of the control analyzer, which is isolated from the incoming plasma, cannot be stressed enough for plasmas similar to those in TELS. Its use helps us to eliminate uncertainties that would otherwise drastically change the results.

C. Space charge limitation

Due to the high densities and fluxes incident on targets in the TELS device, one of the greatest challenges to properly determining the ion information comes in the form of the space-charge limiting current. Because the electrons are sufficiently repelled by the charge on the first grid, an ion beam is formed and creates a new potential arrangement, which, with a high enough density, has the ability to overcome the electrostatic fields generated at the grids. This negates any collected ion information since the potential structure within the analyzer is no longer well-defined. The maximum allowable current density governed by this phenomenon is given by[18]

$$j_{sc,crit} \approx 3.85 \times 10^{-8} \left[(qV_{G3} + E_{\|})^{3/2}/(z - z_m)^2\right] \left[1 + 0.0247 T_i^{1/2} (qV_{G3} + E_{\|})^{-1/2}\right], \quad (4)$$

where $j_{sc,crit}$ is in A cm^{-2}, V_{G3} (the voltage applied to the electron suppressor grid) is in V, $E_{\|}$ is the average ion energy in eV ($E_{\|} \cong T_i + qV_{sheath}$), T_i is the measured ion temperature in eV, q is charge on the ion, and $z - z_m$ is the minimum on-axis distance between the positions within the analyzer that correspond to the minimum and maximum potentials. Using the parameters defined by the RFEA geometry, the expected ion energy values for the TELS system, and the methodology outlined in Ref. 12, the critical space charge limiting current is nearly 520 μA cm^{-2}. This value was calculated assuming that the $z - z_m$ value is, conservatively, the distance between the electron repeller grid and the collector; however, it is more likely the case that this distance would be between the electron repelling and ion discriminating grids since over this distance ions are decelerated from their highest energy (which occurs at or directly past the electron repelling grid). Assuming the beam expands to the diameter of the collector, the limiting current is approximately 2 mA. The maximum current collected by the open analyzer was less than 500 μA (illustrated in Fig. 3), meaning that space charge is not likely to affect

the ion current. If beam expansion was not considered, then experimentally collected currents would greatly exceed this space charge limitation. The beam expansion assumption is considered valid, however, for this case, since at a fringe field of 300 G and an ion temperature of 25 eV, the ion Larmor radius is approximately 1.7 cm. Based on these calculations, the analyzer is likely not space charge limited; however, the fact that the RFEA ion current in Fig. 5(a) appears to never reach a saturation value may indicate a minor influence from the space charge effect.[19,20] If space charge does play a role, the effect seems to be time-dependent since the initial linear drop vanishes as the plasma pulse continues to interact with the analyzer. The degree to which space charge may or may not influence this analyzer is unclear; however, the empirically determined shift potential described in Fig. 5(a) aligns well with the plasma and electron information in Ref. 8, supporting the claim that this effect has minimal influence, if at all.

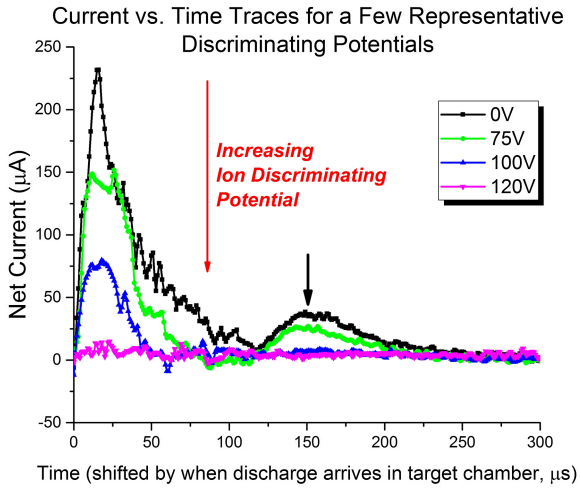

FIG. 4. A comparison of the currents collected at different discriminating potentials for the time domain in which the plasma has reached the target chamber and is interacting with the analyzer. The black arrow again indicates the secondary feature, generated by the associated portion of the PiP profile illustrated in Fig. 3(a).

IV. RESULTS

The results presented are useful in understanding the degree to which the theta pinch heats the ions. At the same axial position in the target chamber, the collected ion currents were compared when using the theta pinch in conjunction with the pre-ionizing coaxial accelerator and when using only the coaxial accelerator.

To determine the net current collected, the current trace of the closed analyzer must be subtracted from the current trace of the open analyzer in order to get rid of the noise generated by electromagnetic and grounding issues. Two representative traces with respect to time can be seen in Fig. 3, where the black trace represents that of the open analyzer and the blue and red represent that of the closed analyzer. The resultant net current trace can also be seen in Fig. 3.

Net currents were then compared as a function of increasing discriminating potential. The shift in the energy distribution is due to the difference between the sheath drop felt at the collimator and the potential at which the collector is held. A plot of the currents over time can be seen in Fig. 4, where the initial negative part of the pulse explained in Fig. 3 is left out. In all cases, this negative current observed due to the transit time of the high energy electrons is no longer observed nearly 60 μs after the PiP initially discharges.

These data in Fig. 4 illustrate that in addition to the primary current peak, there is a second ion peak that occurs approximately 150 μs after the first peak. This current is not an artifact and can easily be explained in reference to Fig. 3, which illustrates typical TELS discharge parameters. Knowing the velocity of the plasma from Ref. 8, it can be safely assumed that the mean time of flight of the plasma is approximately 60 μs. This, however, is the time of flight in reference to the first of two primary plasma structures of interest (denoted in Fig. 3 by the positive peaks in the PiP current profile) that

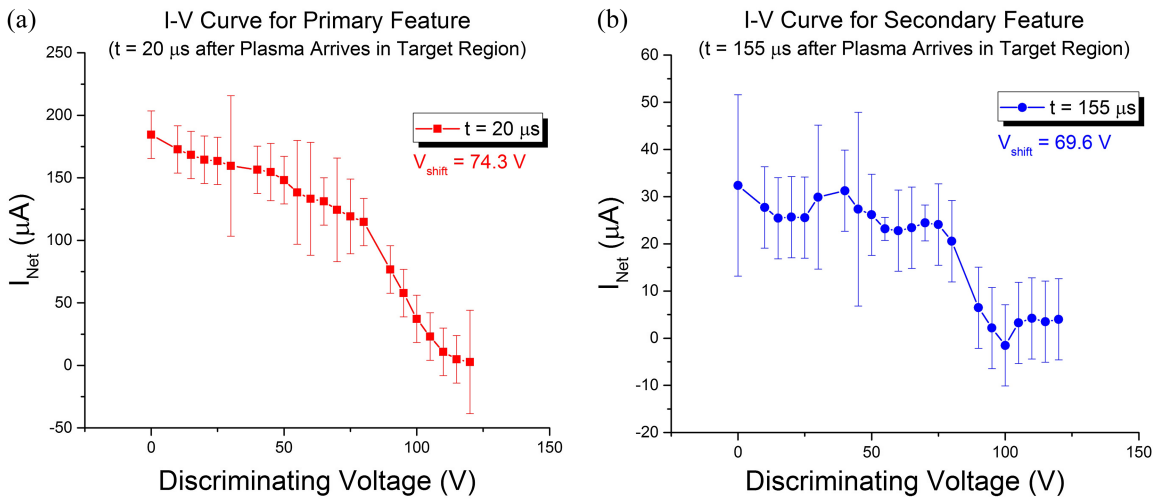

FIG. 5. (a) Currents relative to the ion discriminating potential for the primary feature. The collected current appears to never reach a saturation value, which may be caused by the minimal influence of the space charge effect,[19] the sheath expansion effect,[17,21] or a combination of both. (b) Currents relative to the ion discriminating potential for the secondary feature. Error here represents the standard deviation for multiple shots taken at a single discriminating voltage.

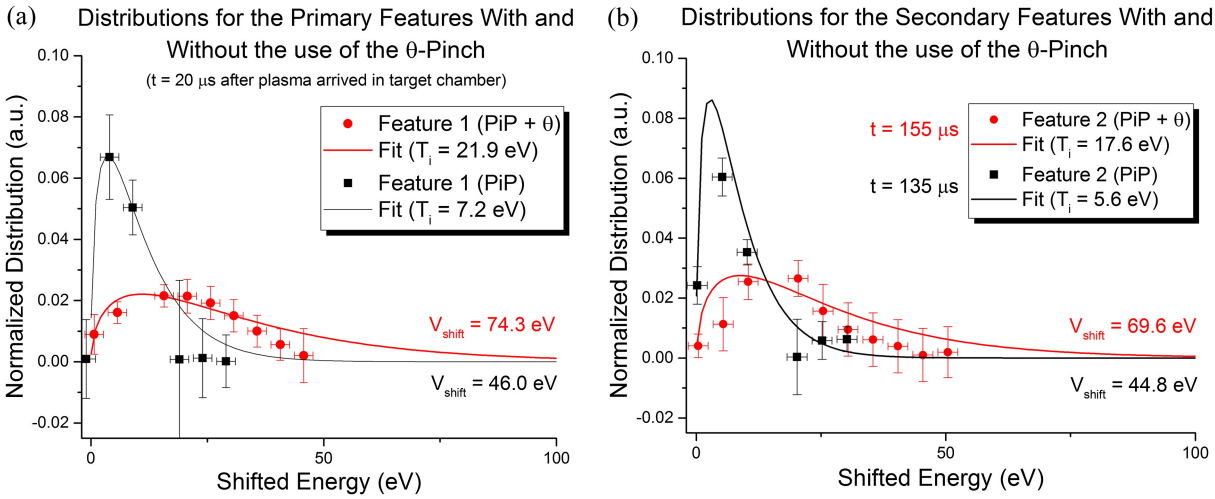

FIG. 6. (a) Comparing the examples of the primary features for each discharge type. The fit T_i value for the PiP + θ pinch was found to be 21.9 ± 3.2 eV, while the fit T_i for the PiP only was found to be 7.2 ± 0.4 eV. (b) Comparing examples of the secondary features for each discharge type. The fit T_i value for the PiP + θ pinch was found to be 17.6 ± 3.4 eV, while the fit T_i for the PiP only was found to be 5.6 ± 1.0 eV. Each distribution has been shifted by its respective shift potential, V_{shift}.

have the appropriate polarity to propagate down the length of the chamber. It is with reference to this initial plasma discharge that the theta pinch fires (set to fire 30 μs after the rise of the PiP current reaches a threshold of 60 kA). This pinch sufficiently compresses the primary plasma structure propagating through the theta region but acts as somewhat of a barrier to the secondary portion of the discharge that has the correct polarity to self-propagate toward the target chamber. The coupling of the lower velocity of the secondary discharge along with the magnetic drag felt by this discharge as it propagates through the theta pinch region easily lends credibility to this second feature seen at 150 μs being due to the second pulse from the PiP.

While the data depicted in Fig. 4 are indicative of how the collected current waveforms decrease with increasing discriminating potential over time, this figure does not readily portray the curves used to relate the collected current to probe theory. The data in Fig. 5 are the currents collected at snapshots in time near the two peaks seen in Fig. 4, plotted as functions of the ion discriminating potential. These data show that the currents in relation to the discriminating potential follow the expected probe traces.

From the plots seen in Fig. 5, these data allow for energy distributions to be found. As described in probe theory (Ref. 17), the derivative of the current with respect to the discriminating voltage is directly proportional to the distribution and can be used to extract ion temperature values. Plots were shifted in time to observe the key features as they interact with the analyzer. This means that the case with the PiP and theta pinch was shifted by 60 μs with respect to the PiP discharge and the case with just the PiP was shifted by 70 μs with respect to the PiP discharge. Distributions were shifted by their respective drifted energy values, evident in the example plots in Fig. 5. The plots can be found in Fig. 6.

The plots in Fig. 6 illustrate representative distribution analyses at individual snapshots in time. The images are meant to draw a comparison between the use and non-use of the theta pinch, but are only taken from individual instants during a plasma pulse. The shapes of the distributions, however, are indicative of the data from the two primary features in each pulse type. On the abscissa, the ion energies are shifted with respect to the experimentally observed shift potentials, as described in Eq. (2). Averaging the analyzed ion energies over the characteristic times for each of the two key features, the signal showed an ion temperature of 23.3 ± 6.6 eV for the first peak and 17.6 ± 1.9 eV for the second peak, when using the theta pinch. Using similar averaging, the signal showed an ion temperature of 7.9 ± 1.1 eV for the first peak and 6.6 ± 0.8 eV for the second peak, without the use of the theta pinch.

V. CONCLUSIONS

Measurements of the ion temperature were carried out using a retarding field energy analyzer (RFEA) in the ThermoElectric-driven Liquid-metal plasma-facing Structures (TELS) pulsed linear plasma source. Two analyzers were used, one open to the plasma and one shielded from the plasma, in order to eliminate hard-to-define electromagnetic effects on the in-vacuum transmission and collection lines. The novelty in using a control analyzer to sample the noise present during the same plasma pulse is due to the transience of TELS, and the importance of such a system cannot be stressed enough since pulsed magnetized plasmas like those generated in TELS can generate currents that would otherwise greatly perturb the collection signal. Ion information was collected from two key features, evident in discharges with and without the use of the theta pinch. Ion temperatures and Maxwellian distributions were assessed, and time-averaged values for these two key features were compared with regards to the use of the theta pinch. While the collected currents for these features may be affected by space charge and sheath expansion effects to some degree, these effects appear to be time-dependent and minimal, especially when comparing key information about the plasma to the material reported in Ref. 8. The degree to which these effects

play a role in measurement will be the topic of future endeavors. Prior to measurement, the hypothesis was that the theta pinch would preferentially impart energy to the ions, thereby heating the plasma. When discharging the theta pinch, the measured ion signal showed an ion temperature of 23.3 ± 6.6 eV for the first peak and 17.6 ± 1.9 eV for the second peak. These temperatures were found by averaging the values for the duration of each of the key features. When only using the PiP, the measured signal showed feature-averaged ion temperatures of 7.9 ± 1.1 eV for the first peak and 6.6 ± 0.8 eV for the second peak. This difference, by approximately a factor of 3, indicates the level with which the theta pinch can effectively and preferentially impart energy on the ions, thus, making TELS one of the few linear, pulsed plasma sources whereby moderately energetic ions strike targets without the need for sample biasing.

ACKNOWLEDGMENTS

This work was supported by the Department of Energy, Contract No. DEFG02-99ER54515.

[1]Y. Yuan, J. Du, M. Wirtz, G.-N. Luo, G.-H. Lu, and W. Liu, "Surface damage and structure evolution of recrystallized tungsten exposed to ELM-like transient loads," Nucl. Fusion **56**, 036021 (2016).
[2]D. P. Boyle, R. Maingi, P. B. Snyder, J. Manickam, T. H. Osborne, R. E. Bell, B. P. LeBlanc, and NSTX Team, "The relationships between edge localized modes suppression, pedestal profiles and lithium wall coatings in NSTX," Plasma Phys. Controlled Fusion **53**, 105011 (2011).
[3]D. N. Ruzic, W. Xu, D. Andruczyk, and M. A. Jaworski, "Lithium-metal infused trenches (LiMIT) for heat removal in fusion devices," Nucl. Fusion **51**, 102002 (2011).
[4]M. J. Baldwin, R. P. Doerner, S. C. Luckhardt, and R. W. Conn, "Deuterium retention in liquid lithium," Nucl. Fusion **42**, 1318 (2002).
[5]R. Majeski, S. Jardin, R. Kaita, T. Gray, P. Marfuta, J. Spaleta, J. Timberlake, L. Zakharov, G. Antar, R. Doerner, S. Luckhardt, R. Seraydarian, V. Soukhanovskii, R. Maingi, M. Finkenthal, D. Stutman, D. Rodgers, and S. Angelini, "Recent liquid lithium limiter experiments in CDX-U," Nucl. Fusion **45**, 519 (2005).
[6]S. Jung, M. Christenson, D. Curreli, C. Bryniarski, D. Andruczyk, and D. N. Ruzic, "Development of a high energy pulsed plasma simulator for the study of liquid lithium trenches," Fusion Eng. Des. **89**, 2822 (2014).
[7]S. Jung, V. Surla, T. K. Gray, D. Andruczyk, and D. N. Ruzic, "Characterization of a theta-pinch plasma using triple probe diagnostic," J. Nucl. Mater. **415**, S993 (2011).
[8]S. Jung, "Development of high energy pulsed plasma simulator for plasma-lithium trench experiment," Ph.D. dissertation (University of Illinois at Urbana-Champaign, 2014), http://hdl.handle.net/2142/50746.
[9]S. Jung, D. Andruczyk, and D. N. Ruzic, "Laboratory investigation of vapor shielding for lithium-coated molybdenum in Devex," IEEE Trans. Plasma Sci. **40**, 730 (2012).
[10]I. S. Nedzelskiy, C. Silva, H. Figueiredo, H. Fernandes, and C. A. F. Varandas, "Compact retarding field energy analyzer for the tokamak ISTTOK boundary plasma," Rev. Sci. Instrum. **77**, 10E729 (2006).
[11]P. Tamain, M. Kočan, J. Gunn, A. Kirk, J.-Y. Pascal, and M. Price, "Ion energy measurements in the scrape-off layer of MAST using a retarding field analyzer," J. Nucl. Mater. **415**, S1139 (2011).
[12]R. A. Pitts, R. Chavan, S. J. Davies, S. K. Erents, G. Kaveney, G. F. Matthews, G. Neill, J. E. Vince, I. Duran, and JET-EFDA Workprogramme Contributors, "Retarding field energy analyzer for the JET plasma boundary," Rev. Sci. Instrum. **74**, 4644 (2003).
[13]D. Brunner, B. LaBombard, R. Ochoukov, and D. Whyte, "Scanning retarding field analyzer for plasma profile measurements in the boundary of the Alcator C-Mod tokamak," Rev. Sci. Instrum. **84**, 033502 (2013).
[14]Y. C. Francis Thio, R. Eskridge, M. Lee, J. Smith, A. Martin, T. E. Markusic, and J. T. Cassibry, "An experimental study of a pulsed electromagnetic plasma accelerator," in *38th AIAA/ASME/SAE/ASEE Joint Propulsion Conference and Exhibit* (AIAA, 2002), pp. 2002–4269.
[15]Z.-G. Shen, C.-H. Liu, C.-H. Lee, C. Wu, and S. Yang, "A study of a coaxial plasma gun," J. Phys. D: Appl. Phys. **28**, 314 (1995).
[16]K. F. Schoenberg, R. A. Gerwin, R. W. Moses, Jr., J. T. Scheuer, and H. P. Wagner, "Magnetohydrodynamic flow physics of magnetically nozzled plasma accelerators with applications to advanced manufacturing," Phys. Plasmas **5**, 2090 (1998).
[17]I. H. Hutchinson, *Principles of Plasma Diagnostics*, 2nd ed. (Cambridge University Press, 2002).
[18]A. W. Molvik, "Large acceptance angle retarding-potential analyzers," Rev. Sci. Instrum. **52**, 704 (1981).
[19]D. Brunner, B. LaBombard, R. Ochoukov, R. Sullivan, and D. Whyte, "Space-charge limits of ion sensitive probes," Plasma Phys. Controlled Fusion **55**, 125004 (2013).
[20]D. Grondona, H. Kelly, and A. Márquez, "Spatial charge effects in retarding field analyzer ion measurements in a cathodic vacuum arc," Appl. Phys. Lett. **79**, 317 (2001).
[21]H. K. Fang and C. Z. Cheng, "Retarding potential analyzer (RPA) for sounding rocket," in *An Introduction to Space Instrumentation*, edited by K. Oyama and C. Z. Cheng (Terrapub, 2013), pp. 139–153.